Journal of Water Process Engineering 44 (2021) 102413

Contents lists available at ScienceDirect

Journal of Water Process Engineering

journal homepage: www.elsevier.com/locate/jwpe

Enhanced removal efficiency of heavy metal ions from wastewater through functionalized silicon carbide membrane: A theoretical study

Sina Karimzadeh [a], Babak Safaei [a,b,*], Tien-Chien Jen [a,*], Peter Ozaveshe Oviroh [a]

[a] Department of Mechanical Engineering Science, University of Johannesburg, Gauteng 2006, South Africa
[b] Department of Mechanical Engineering, Eastern Mediterranean University, Famagusta, North Cyprus, via Mersin 10, Turkey

ARTICLE INFO

Keywords:
Purification
Wastewater
Heavy metal ions
SiC Membrane
PMF

ABSTRACT

Development and designing of heavy metal ion separation systems from wastewater play a essential role in environmental protection. For this purpose, in this research, we modeled the synthetic wastewater samples and investigated the capabilities of nano-porous silicon carbide membranes (SiC) with fluorine, nitrogen, and hydroxyl-atom decorated pores under hydrostatic pressures. Increase of applied pressure on SiC with larger pore diameters had more intense effects on water flux and ion rejection. It was also found that, due to different electronic properties of decorated atoms in the edge of pores, which played important roles in their interactions with water molecules and metal ions, as well as energy barrier and permeation, water flux and ion injection were improved. The potential of mean force (PMF) calculation showed that the energy barrier for passing through functionalized pores was higher for metal ions and lower for water molecules. The presence of functional groups in the edge of SiC pores provided selective ion rejection property which was highest for Zn^{2+} ions. PMF analysis results proved that the PMF values of metal ions were in the following comparative order: SiC@F>SiC@N>SiC@OH>SiC. It was also observed that increase in temperature significantly increased water flux and decreased ion rejection. Also, SiC membrane separation systems improved ion rejection in the presence of electric field along the opposite direction of piston movement, which was more intense in functionalized membranes and results indicated that in voltage of 200 mV/Å had the best ion rejection of about 98%.

1. Introduction

Purification and reusing of water from secondary effluents is becoming a more appealing approach to the growing problems of water shortage and deterioration of water quality [1]. Thus, water treatment systems that are multifunctional, compact, flexible, resilient, chemical-free, and energy-efficient are needed to address global water shortage and water pollution [2]. Since water is an essential part of our everyday lives, effective treatment technologies are required to clean and recycle water [3]. Osmotic pressure-driven membranes have recently attracted increased interest in water and water purification due to their lower energy consumption compared to other available methods [4]. Multi-stage flash (MSF), multi-effect distillation (MED), and reverse osmosis (RO) are some of the most commonly used processes in water treatment/desalination; however, RO is gaining greater market share [5–7] due to its lower energy consumption. RO water treatment process entails applying pressure to feed water to push freshwater molecules through a permeable membrane, filtering ions and other contaminants in the process while allowing freshwater to pass through [7–9].

Several membrane types such as thin-film composite (TFC) materials [10–12], ceramics [13–15], nanotubes [16,17], and two dimensional (2D) structures such as boron nitride (BNNS) [18], MXene [19], MoS_2 [20] and zeolites [21] are used in RO for drinking water purification as well as wastewater treatment and reuse. These play important roles in supplying reliable and safe water, mitigating adverse environmental effects, and providing water availability [22]. despite the advantages of nanoporous membranes in water desalination such as high-water permeability and ion rejection, they have a some disadvantages. There are some vital elements in water that are beneficial to human health. Removing all ions from water is one of the disadvantages of this materials that led many scientists to use other methods to compensate for this issue.

Among ceramic 2D membranes, SiC has a honeycomb structure which composed of silicon and carbon atoms [23]. Similar to graphene structure, SiC with Si and C atoms use sp2 hybridization. Lin et al. synthesized SiC nanostructure experimentally [24]. The double bonds

* Corresponding authors at: Department of Mechanical Engineering Science, University of Johannesburg, Gauteng 2006, South Africa.
E-mail addresses: skarimzadeh@uj.ac.za (S. Karimzadeh), babak.safaei@emu.edu.tr (B. Safaei), tjen@uj.ac.za (T.-C. Jen), poviroh@uj.ac.za (P.O. Oviroh).

https://doi.org/10.1016/j.jwpe.2021.102413
Received 3 September 2021; Received in revised form 25 October 2021; Accepted 26 October 2021

between C and Si are sp2 bonding type because Si atoms has a high covalent radius and cannot form π- bonding. Materials with honeycomb structure and aromatic rings have great electron density that hinders ions and molecules permeation. SiC has emerged as an excellent porous material for the treatment of wastewater owing to its advantages over more widely used polymeric membranes in terms of higher flux, improved separation properties, longer working life, fouling resistance, and smaller footprints [25–27]. In addition to these attributes, high chemical stability over the whole pH range, good thermal resistance, good mechanical strength, high hardness feature, and outstanding hydrothermal stability can be mentioned [28–30]. using SiC in metal ion separation applications, nano pores must be created by drilling in its structure with eliminating C and Si atoms. The chemically functionalizing of pores in SiC membrane, could have a uniqe feature and different applications [31].

Chemical vapor deposition (CVD) is being used for the fabrication of SiC [32-34]. However, there is a need for the deposition of SiC at low temperatures on surfaces with high aspect ratios [35], which can be achieved using atomic layer deposition (ALD) process [36]. Several methods including ion irradiation [37], chemical etching [38], electron beam [39], and helium bombardment [40] are being used for creating pores in membranes. However, ALD can also create functionalized pores [41].

In experimental works, numerous methods such as adsorption, ion exchange, chemical precipitation, and membrane filtration have been utilized to separate heavy metal ions [42]. Furthermore, some experimental works were carried out, on integrating pore into nanosheets. Ion bombardment is one of the methods for creating pore in nanosheets [43]. To give new characteristics to materials, chemical functional groups such as -F, -N, -OH and etc, could be introduced on materials [44]. Lin et al. [45] created pores in BNNS by using ball milling method. Then, for functionalizing, They used long alkyl chain amine, which resulted in the creation of an acid-base interaction between amine groups and BNNS surface. These functional groups could be influential in separation processes. Also, many experimrntal studies claimed that the pores could functionalized with different atoms in membranes [46–48].

Moreover, with functionalizing the edge of pores, despite adjusting pore size, the selective separation capability of the nano-porous membrane could be enhanced. Cohen-Tanugi et all designed functionalized graphene for purification of salted water [49]. They investigated the purification performance by considering pore size; different applied reverse osmosis pressure, and chemical functionalization.

In a study by Das et al. [50] on the permeability behavior of silicon carbide-based membranes, a membrane with porosity ~48 vol% and mechanical strength 31.5 MPa showed water permeability of 13 298 $Lm^{-2}h^{-1}bar^{-1}$. On the other hand, Chen et al. [34] used chemical vapor deposition to study the effect of tuning pore size. Due to a combination of hydrophilic and charge interactions, the formed SiC-deposited ultrafiltration membranes showed low fouling characteristics and slight permeance losses during oil-in-water emulsion filtration. Furthermore, Wit et al. [51] used SiC to develop a highly permeable and mechanically robust hollow fiber membrane with a very high water permeability of 50,000 L m^{-2} h^{-1} under 1 bar pressure difference. However, apart from high permeability, the selectivity of these membranes also needed great attention. In addition to pollutants, heavy metal ions such as Zn^{2+}, Pb^{2+}, and Cd^{2+} are other forms of harmful pollutants that can easily pass through membranes used in wastewater treatment.

Functional groups attached to the pore edges of membranes are another important factor in the water treatment process. In the water treatment process, hydrophobic and hydrophilic functional groups have different effects [52,53], thus allowing the applications of pore chemistry beyond filtration [54]. Pore chemistry plays an vital role in changing water flux [55]. Several methods have been applied in the functionalization of SiC for different purposes [56–58]. Adding different functional groups to the edges of formed pores results in more stable and highly permeable membranes [59,60].

Applying electric fields is an innovative method to solve the discussed disadvantage. Also, It can be effective in water desalination processes and water transportation. Recently in many studies, utilized electric field for nanofluid transport through nanostructures was investigated. Li et al. drive the water through nanotube by applying electromagnetic field in rotating manner [61]. Also, Theoretical investigation in effect of electric fields on the water flow rate in the carbon nanostructures was reported [62]. In another work the significance of external electric field direction in water flow rate through nanochannel was studied [63]. Meanwhile, as our best knowledge, no similar work has been ever done in the literature to date to investigate the water desalination performance with different functionalized SiC nanostructure and with different ions type under applied electric field and pressure.

To the best of our knowledge, no experimental or theoretical study has been reported in the literature on the removal of (Zn^{2+}, $Pb^{2+,}$ and Cd^{2+}) heavy metal ions by functionalized SiCs. Hence, in the present work, molecular dynamics (MD) and density functional theory (DFT) simulations were performed to study the effects of -F, -N, and -OH functional groups on water flux and ion rejection under different hydrostatic pressures. Because of their important role in the interactions of water molecules and ions. In addition, an electric field was applied to study its effects on ion permeation. Furthermore, we also studied water flux as functions of pore size, applied hydrostatic pressure, ion rejection, and energy barrier using PMF. Overall we tried to provide an understanding of the role of functionalized group at pore of SiC in the water treatment process.

2. Simulation methodology

In this study, the possibility of the elimination of Cd^{2+}, Pb^{2+} and Zn^{2+} heavy metal ions using silicon carbide (SiC) membrane with functionalized pores under reverse osmosis has been investigated through DFT and molecular dynamics (MD) simulations. Cd^{2+}, Pb^{2+} and Zn^{2+} have different atomic weights (112.41, 207.2 and 65.38 u, respectively), and each metal ion was dissolved in water at the same molecular concentration (0.6 mol. L^{-1}). In many similar works, heavy metal ion concentrations in aqueous solutions have been examined in the assumed range [64–67]. In this research, we used porous SiC membranes, that pores decorated with F, N and OH functional groups to customize the physical and mechanical properties of membrane pores. In the following section, the effects of temperature and applied electric field on the efficiency of ion separation of the membranes are discussed.

The designed synthetic wastewater system contained a porous SiC membrane, above which aqueous solutions of heavy metal ions were placed, and to apply reverse osmosis pressure, graphene membranes were used on both sides of SiC membrane which acted as pistons to keep the solutions under fixed pressure. It is noted mentioning that to maintain experimental conditions, the piston on the other side was exposed to atmospheric pressure of 1 bar. The dimensions of the simulated system were 61×58×200 Å along x, y and z axis, respectively. The solution under the piston contained 8426 water molecules that TIP3P model [68] was applied for the prediction of interactions of water molecules. Then, 50 heavy metal ions of each Cd^{2+}, Pb^{2+} and Zn^{2+} along with 300 corresponding salt ions (Cl^{-1}) were randomly added and distributed into water using Packmol software [69]. Atomic charges of the systems were considered to be neutral. The overall diagram of the system is presented in Fig. 1. The surface area of the SiC membrane was 61 Å×58 Å. In the simulation systems, the porosity concentration of SiC was considered 9.5% that contained four same pores. The pristine SiC contained 734 atoms and to create pores, 6 Carbon atoms and 7 Silicon atoms were eliminated and the corners of the pores were engineered by F, N and OH functional groups.

In this study, to obtain precise results resembling those obtained under laboratory conditions, all porous SiC membrane structures were

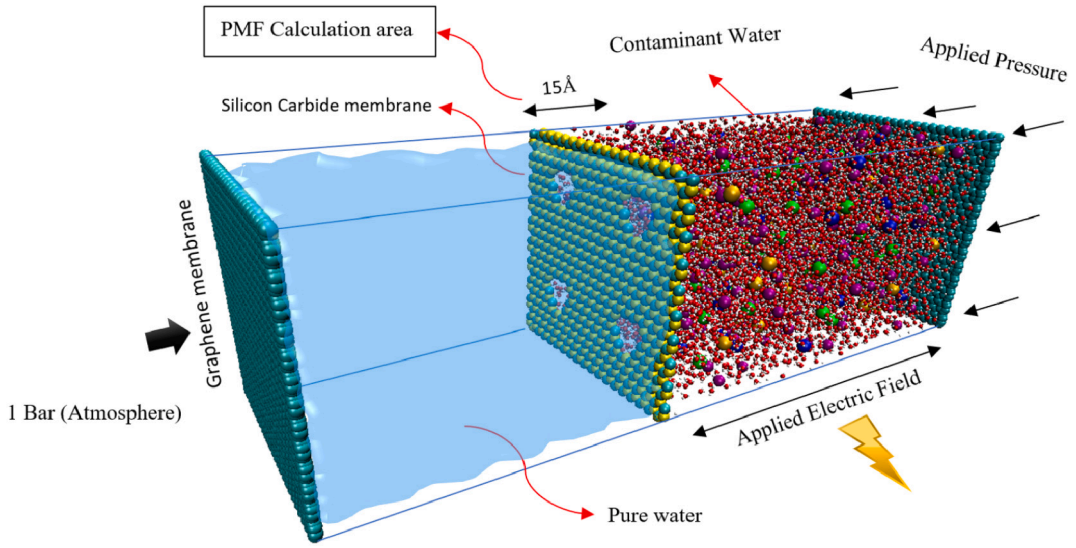

Fig. 1. Schematic diagram of the simulation system consisting of one SiC membrane modified with four pores in the middle and two graphene membranes (cyan) as pistons. The right-side chamber contained contaminated water with heavy metal ions under high pressure and electric field and the left-side chamber contained pure water under 1 atm pressure (O in red, H in white, Cd^{2+} in orange, Pb^{2+} in blue, Zn^{2+} in green and Cl^{1-} in purple).

optimized using B3LYP/6-31+G(d,p) method [70] after designing and before MD simulation. Then, DFT output structures were used in MD simulation systems. Also, partial charges of atomic structures were obtained using DFT calculation results. Fig. 2 shows different optimized structures with engineered pores that were studied in this work. Also, Table 1 summarizes the geometric and electronic properties of studied models. All DFT calculations were performed using Gaussian 9.0 package [71].

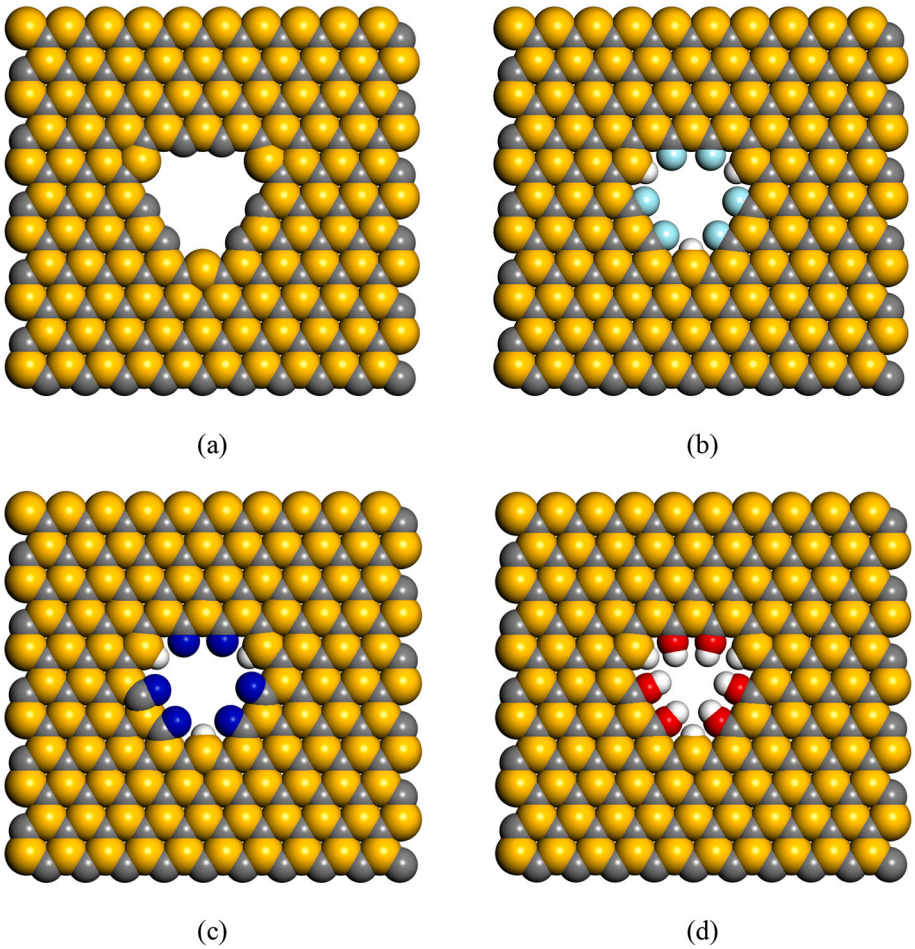

Fig. 2. Schematic diagrams of four differently decorated SiC membranes a) pristine SiC b) SiC@F c) SiC@N d) SiC@OH

Table 1
Lennard-Jones parameters and partial charges for all atom types

Atom type	$\epsilon\left(\frac{Kcal}{mol}\right)$	σ (Å)	Partial charge
C [SiC]	0.070	3.985	-1.67
Si [[SiC]	1.664	0.469	+1.67
C [graphene]	0.070	3.985	0
N [SiCN]	0.072	3.716	-0.256
H [SiCN]	0.022	2.640	-0.172
F [SiCF]	0.135	3.260	-0.390
H [SiCF]	0.022	2.640	-0.150
O [SiCOH]	0.152	3.540	-0.670
H [SiCOH]@(O)	0.046	0.449	+0.456
H [SiCOH]@(Si)	0.022	2.640	-0.158
O [water]	0.152	3.536	-0.734
H [water]	0.046	0.449	+0.417
Cd^{+2}	0.00597	2.70	+2
Pb^{+2}	0.19112	3.00	+2
Zn^{+2}	0.250	1.950	+2
Cl^{-1}	0.118	4.420	-1

To evaluate the efficiency of the membranes in the separation of heavy metal ions as well as water permeability, different pressures of 25, 50, 100, 150 and 200 MPa were applied along Z direction using graphene piston onto the solution-containing section of the system and the other section was kept under 1 atm pressure. Then, the amount of penetrated particles in the refined section was monitored throughout the simulation. To prevent the movement of central SiC membrane along the direction of pressure, it was fixed during the simulation. It is worth mentioning that graphene pistons were fixed on both sides of the system along x and y axis but could move by applying pressure along z axis. The partial charge of carbon atoms in graphene pistons is considered zero. All MD simulations were performed using LAMMPS package [72,73] and VMD software [74] was used for visualization of simulated systems. Before the simulation and in order to decrease the energy level of the simulated systems, minimization was performed. Then, in the equilibrium stage, systems were equilibrated for 1 ns using Nose-Hoover barostat and thermostat algorithm under constant canonical ensemble temperature of 298 K and pressure of 1 atm. Time steps were considered to be 0.1 fs, and simulation duration time was 5 ns.

Tersoff force field for C and Si atoms in graphene and SiC membranes were defined and functional groups were modeled using Lennard-Jones potential in which force-field parameters were obtained from reference [65]. Table 1 summarizes all 6-12 Lennard jones parameters for atoms in the structures. Lorentz-Berthelot mixing rule [75] was applied for all pairwise L-J terms between unlike particles. L-J interaction cutoff was considered 12 Å. Long-range electrostatic interaction were calculated using Particle Mesh Ewald [76]. Periodic boundary conditions was applied along all directions.

Nonbonded interactions among heavy metal ions and water molecules with SiC and graphene membranes were expressed as [77]:

$$U_{nonbond} = 4\epsilon_{ij}\left[\left(\frac{\sigma_{ij}}{r_{ij}}\right)^{12} - \left(\frac{\sigma_{ij}}{r_{ij}}\right)^{6}\right] + \frac{q_i q_j}{4\pi\varepsilon_0 r_{ij}} \quad (1)$$

where ϵ_{ij} and σ_{ij}, respectively, are energy and length of Lennard-Jones potential. q_i, q_j denotes charges on i and j atoms, respectively, r_{ij} is center to center distance, and ε_0 is dielectric permittivity constant.

All bonding and stretching interactions were modeled using harmonic potentials as [78]:

$$U_{bond} = \frac{1}{2}k_r\left(r - r_{eq}\right)^2 \quad (2)$$

$$U_{angle} = \frac{1}{2}k_\theta\left(\theta - \theta_{eq}\right)^2 \quad (3)$$

Non-bonded cross interaction parameters of unlike pairs were determined by Lorentz-Berthelot mixing rules.

The amount of applied hydrostatic pressure on solvent molecules through the application of force onto each carbon atom in graphene membrane (piston) was stated as [79]:

$$F = \frac{\Delta P \times A}{n} \quad (4)$$

where ΔP is the considered hydrostatic force, and A and n are the surface area and the number of C atoms of graphene piston.

To determine the mechanism of separation through the functionalized pores of SiC, potential of mean force (PMF) [80–82] was calculated as the free energy profile of water molecules and heavy metal ions passing through pores using umbrella sampling method [83]. Umbrella sampling method was applied by considering water molecules or metal ions in simulation cell as probes.

Therefore, in SMD simulations of the investigated samples, water molecules and heavy metal ions were drawn as springs and the work of pulling was calculated as [84]:

$$W = -K\upsilon_z \int_0^t d\acute{t}\left[Z(\acute{t}) - z_0 - \upsilon_z\acute{t}\right] \quad (5)$$

where K, υ_z and z_0 are spring constant, pulling velocity and initial position of molecule, respectively. Then, PMF was calculated using free energy change ΔG on the basis of Jarzynski's equality [85]:

$$\Delta G = -\beta^{-1}\ln[\exp(-\beta W)] \quad (6)$$

where $\beta = k_B T$, $[exp(-\beta W)]$ is ensemble average.

To enhance the accuracy of PMF calculation results, SMD simulations for each water molecule and heavy metal ion in each model were repeated 10 times under initial conditions, accounting for 200 overall simulation runs for calculations. Then, free energy of each ion was obtained through averaging the results obtained for 10 trajectories.

3. Result and discussion

3.1. Geometrical and electronic properties

After designing and preparation of the structures, to optimize the geometry of the structures and obtain the partial charges of atoms in the structure, DFT calculations were performed using Gaussian software. These calculations were performed using B3LYP level of theory and 6-31G+ basis set which have been applied in many research works [86–88]. The partial charges of optimized atoms were determined using Mullekin in the range of (-1.67 ~ +1.67), as given in Table 1. Also, Fig. 3 shows the charge distribution and optimized pore diameters which were found to range from 4.1 to 10.3Å. Then, optimized structures were applied to conduct all simulations.

3.2. Water flux and ion separation performance under different applied pressures

In this study, water flux was equal to the number of water molecules passing through the pores along z-direction in the unit of time. Fig. 4 shows water flux in different systems containing SiC membranes with pores decorated with F, N and OH functional groups under different hydrostatic pressures. Partials charges in SiC and decorated atoms on pore edges could alter resistance to the entrance of water molecules and heavy metal ions, resulting in higher or lower water flux. With the increase of hydrostatic pressure, the mobility of water molecules and the number of contacts were increased, resulting in the passage of water molecules from pores. However, with this change in behavior with pressure increase up to 50 MPa, in functionalized pores unlike pristine ones, due to smaller diameters, no variation was observed in the increasing trend of flux. In all systems, the flux increasing trend was linearly with applying higher pressure. The highest flux in pristine SiC

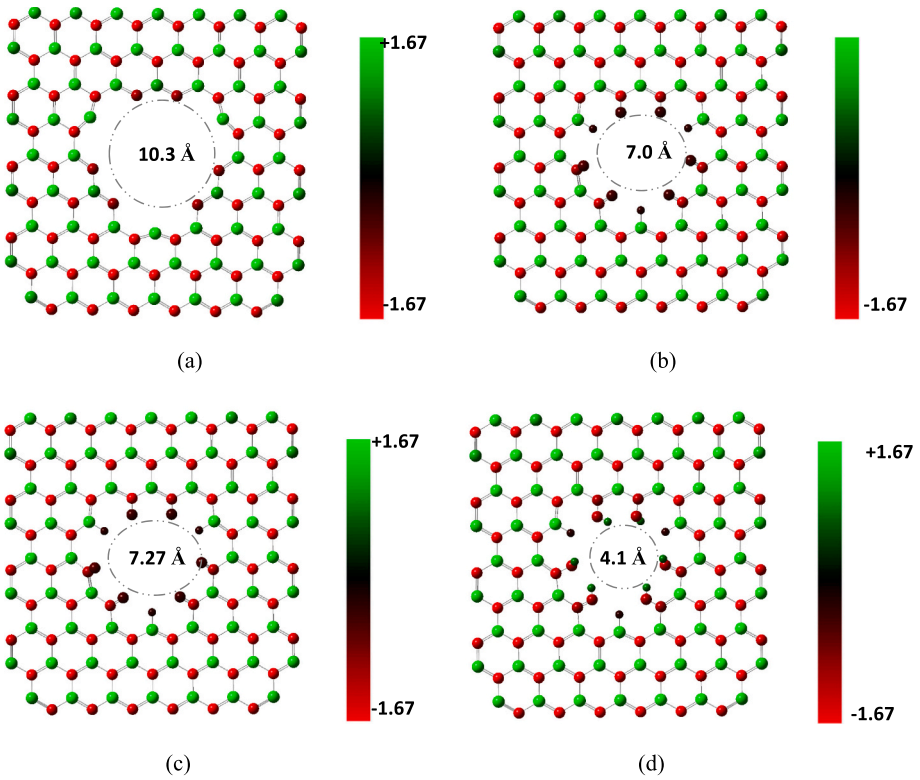

Fig. 3. Optimized pore diameters and Mullekin charges of atoms in decorated SiC membranes a) pristine SiC b) SiC@F c) SiC@N d) SiC@OH

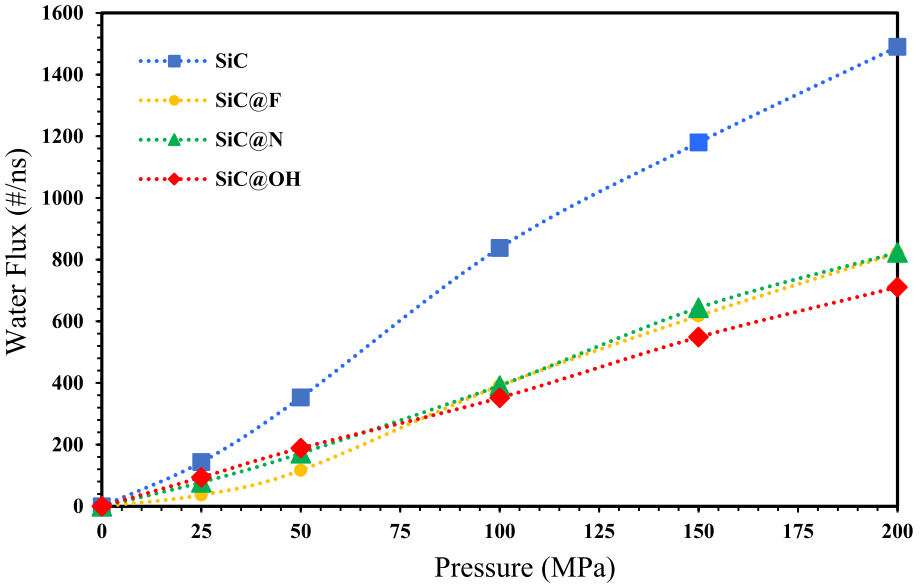

Fig. 4. Water flow rate through different SiC membranes as a function of applied pressure

was due to higher diameters of pores compared to functionalized membranes. The effect of diameter increase on flux rate and ion separation was also reported [89–92]. As shown in Fig. 4, it could be seen that flux rate through SiC@N membrane followed a similar trend to that of SiC@OH to up to 80 MPa. However, at higher pressures, due to stronger effect of hydrostatic pressure, a similar behavior to that of SiC@F was observed which was indicative of similar susceptibility of the two membranes at higher pressures. It is note mentioning that SiC@F membrane let the lowest water flux to up to 50 MPa which indicated non-susceptibility to hydrostatic pressure up to this point. Due to the variations of water flux rate in these membranes, it could be concluded that pore diameter and decorating atom type of the pore were important factors in determining the amount of permeated water molecules.

As can be seen from Fig. 4, the effect of pore chemistry on water flux was more intensive at lower pressures. For example, at 25 MPa, although the pore diameter in SiC model was about~ 2.5 times larger than that in SiC@OH model, there was not much difference in the amount of water flux. In systems with functionalized pores, O atoms in water molecules formed hydrogen bonds with H atoms on pore edges. Also, H atoms of ware molecules formed hydrogen bonds with F, N and O atoms. In this

process, F, N and O atoms acted as electronegative atoms. Negatively charged atoms on pore corners, such as -F, -H and -N, could increase water flux since they cause the attachment of water molecules on both membrane sides, acting as canals to facilitate water flux on both membrane sides. Therefore, decorated atoms on pore corners could affect water flux rate. By increasing pressure, water flux difference between SiC and functionalized models was increased because hydrostatic force prevailed the pore chemistry effect.

Fig. 5 shows total ion rejection percentage for different systems with SiC membranes. For pristine SiC membranes, it was witnessed that at minimum pressure of 25 MPa, heavy metal ions were able to pass through pores 10.3Å in diameter, which indicated 95% ion rejection efficiency. In comparison functionalized membranes at 25 MPa presented 100% ion rejection efficiency. With the increase of pressure to up to 50 MPa, a 13% decrease of ion separation in pristine SiC was observed, while in functionalized membranes, separation trend was almost constant and still above 99%. In functionalized models, with the pressure increase from 50 to 200 MPa, ion rejection was linearly decreased, which was 47, 48 and 38% reduction for SiC@F, SiC@N and SiC@OH membranes, respectively. Nevertheless, for pristine SiC membrane, the linear decreasing manner in ion rejection starts from a lower pressure range from 25 to 150 MPa, which was 72% reduction. Also, at pressures above 50 MPa, due to susceptibility to pressure, difference in the separation trend of functionalized membranes was started. As presented in the curve shown in Fig. 5, SiC@OH membrane had the highest ion separation efficiency in the elimination of heavy metal ions. SiC@OH membrane under 100 MPa presented about 37% ion separation capability and better flux rate than other functionalized membranes. Consequently, the total ions rejection capability of examined SiC membranes for pressure higher than 75 MPa is predominantly related to the size of the pores. In other words, due to the high pressure, the effect of the hydrostatic force in ion rejection overcomes the pore barrier chemistry.

Furthermore, to investigate the efficiency of the selective separation of different ions and influences of functionalized groups, by pristine and functionalized SiC membranes, the system under 100 MPa pressure at 298 K temperature was adopted as the main system. The bar diagram in Fig. 6 presents that pristine SiC membrane separated all four ions almost at similar efficiency due to its low and uniform energy barrier. Zn^{2+} ions was most rejected on functionalized membranes. Higher Zn rejection on SiC@F and SiC@OH membranes is due to higher electronegativity of

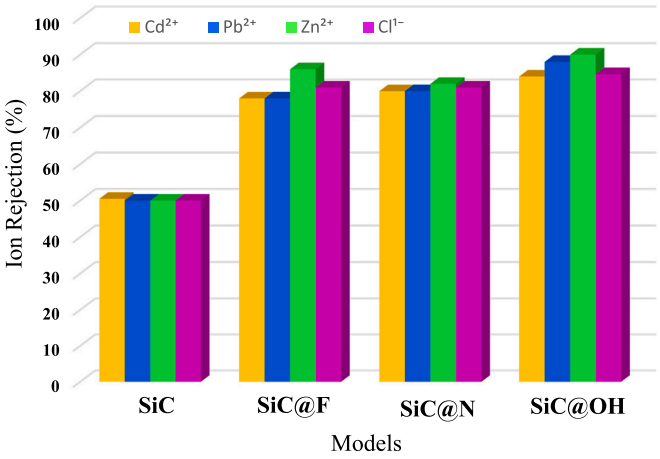

Fig. 6. Heavy metals and Cl^- ions rejections of various SiC membranes under 100 MPa and 298 K

functional atoms F and O on pores and the intrinsic tendency of this ion to have low resistance against the energy barriers of decorated pores. The separation amount of Pb^{2+} and Cd^{2+} ions in systems with SiC@F and SiC@N membranes was almost similar due to similar pore diameter, while in system with SiC@OH membrane, separation of Pb^{2+} was about 4% higher than Cd^{2+}, due to lower pore diameter, the effects of functional groups became more appearant. This behavior indicated lower resistance of Pb^{2+} ions compared to Cd^{2+} ions against energy barrier of pores decorated with -OH functional group.

Fig. 7 shows the number of filtered water molecules during 5 ns simulation time for four examined systems with different SiC membranes. As was seen in pristine SiC membrane, water molecules had passed through pores at much higher rates than functionalized pores due to larger diameters and lower energy barrier. Comparison of the number of permeated molecules at the end of simulation showed that flux rate was directly related to pore diameter. However, comparison of these data at the beginning of simulation showed that SiC@OH functionalized membrane, despite smaller pore diameters than the pores on other models due to the presence of hydrophilic atoms in decorated OH functional group, water molecules tended to permeate through pores in the absence of hydrostatic pressure. In other words, the presence of

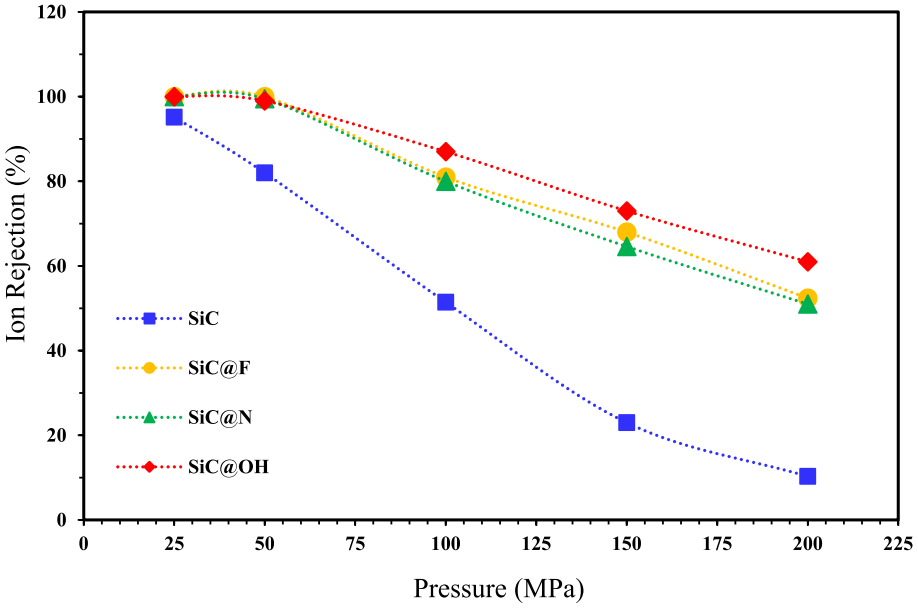

Fig. 5. Total Ion rejection percentage on different SiC membranes as a function of applied pressure

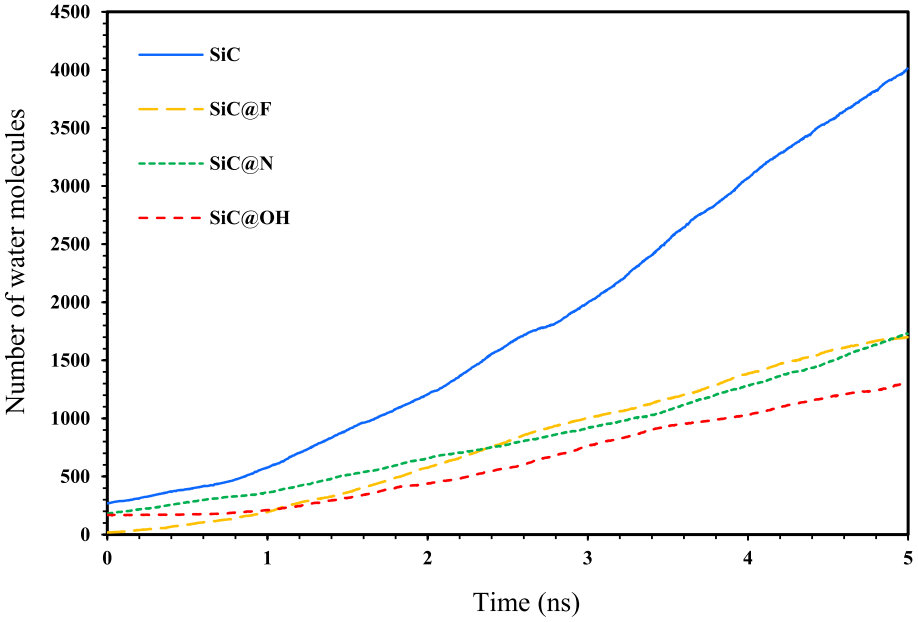

Fig. 7. The number of permeated water molecules in different SiC membranes versus simulation time

hydrophilic atoms on pore edges could act as a molecular bridge to facilitate the permeation of water molecules. Presence of F atoms on pore edges of SiC@F membranes, due to its weaker hydrophilic nature than N atom and OH functional group, presented lower tendency to the permeation of water molecules resulting in stronger dependency on the presence of hydrostatic pressure in these systems. In the diagram shown in Fig. 7, this hypothesis was clearly observed at times above 2.5 ns where high hydrostatic pressure overcame Van der Waals interactions between water molecules and F atoms on the pore edges of SiC@F membrane.

3.3. Water density and velocity distribution

To better understand the mechanism of the permeation of water molecules through designed pores, we investigated the structure of fluids in simulation box along z-axis in the range of -30 < z < 30 under 100 MPa pressure considering the location of pore as zero-point based on the profile of concentration and velocities of water molecules. The results obtained from this section were extracted from the final simulation time of 5 ns. Fig. 8(a)(b) shows concentration profiles of water density and velocity, respectively, for current systems. The peaks on the right side of the figures were assigned to the chamber under high hydrostatic pressure. In Fig. 8(a), as was seen, large peaks appeared in vicinity of membrane and on high pressure side. Due to high Van der Waals interactions among water molecules and SiC atoms on the surface of membrane, water molecules tended to accumulate at this location and form layered water structure. On the other hand, high pressure caused further accumulation of water molecules on high pressure side of the membrane and the difference in the sharpness of peaks compared to those on the left side (low pressure) are evident. It is also note mentioning that water concentration at the center of pore, which contained flux, was the lowest. Fig. 8(b) shows sharper peaks of velocity near the point Z= 0 in low pressure chamber which indicated high velocity of water molecules after being released from high pressure region and passing through the pore. Comparison of the power of concentration peaks for recently studied models showed that the strongest peak was obtained for SiC@OH membrane pore and the weakest concentration peak was obtained for pristine SiC pore with the largest pore diameter.

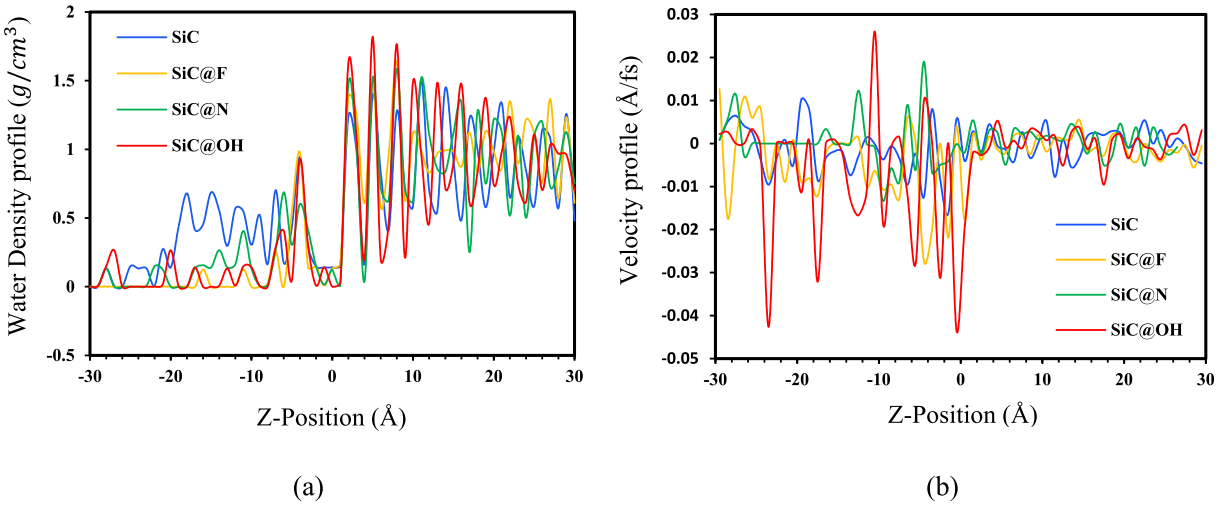

Fig. 8. a) Water density b) water velocity profiles along the z-direction of the box (-30 < z < 30) for all models under 100 MPa and 298 K

Similar trend was also observed for velocity profile. Therefore, it could be concluded that in models containing pores with lower diameters, due to higher permeation barrier and lower flux, water molecules tended to further accumulate near the membrane. Also, the first peaks of SiC@N and SiC@OH membranes appeared at lower distances which indicated stronger Van der Waals interactions among water molecules and N atoms and OH functional group. Average concentration of water in atmospheric pressure (low pressure) side was found to be about 1g/cm^3 which seemed to be reasonable. It is noteworthy that for other systems with different pressures also similar concentration and velocity profiles were obtained.

3.4. Radial distribution function (RDF) of heavy metal ions

In this section, the distribution and behavior of heavy metal ions as a reference and density of hydrogen atoms of water molecules in radial as a function of distance in the solution under 100 MPa pressure at 298 K have been investigated. In Fig. 9, for each of 4 ions, one sharp peak with different intensities appeared. This difference showed that the ions had different hydration numbers. r denotes the closest covalent distance between ion particles and hydrogen atoms of water. The first peak at 2.3Å was assigned to the distance of Cl^{-1} ion from hydrogen atoms of water and was the first hydration shell which was the closest to ion in the range of water molecule. The second and third peaks were related to the hydration shell of Zn^{2+} and Cd^{+2} ions at about 2.95Å and fourth peak at 3.35Å belonged to Pb^{2+} ion. Since the charge of all metal ions was +2, a comparison of peak strengths of these 3 ions revealed that Zn^{2+} and Cd^{2+} ions had larger peaks than Pb^{2+} ion since they had stronger and more stable interactions with Van der Waals interactions with water molecules. This phenomenon resulted in the higher accumulation of these ions, especially Zn^{2+}, with water molecules and therefore, better ion rejection. The findings of this section, as shown in Fig. 6, also proved that Zn^{2+} ions had better ion rejection property. Since this analysis focused on the behavior of ions near water molecules, the type of applied membrane as well as change of pressure and temperature did not affect the obtained results.

Fig. 10 shows the integration of RDF for ion and water indicating the average number of water molecules N_{AB} in hydration shell with distance r from ion center. The value of this parameter was obtained as:

$$N_{AB} = 4\pi\rho \int_0^R g_{(r)} \times r^2 \times dr \quad (7)$$

where ρ, r, *and* $g_{(r)}$ are density, radial distance, and RDF, respectively.

The value of this parameter was found to be 5 to 6 for heavy metal ions and about 8 for chlorine which indicated the number of water molecules surrounding them.

3.5. Potential mean force (PMF) calculation

PMF parameter predicts the possibility of the passage of ions and water molecules by calculating energy barrier exerted onto them while passing the membrane pore. Higher PMF values for a particle indicate higher energy barrier exerted onto it making its passage through the pore more difficult. To do so, first, systems were equilibrated at 298K under atmospheric pressure. In the meantime, metal ions and water molecules were kept at motion start point at 15Å to equilibrate the surrounding water molecules. Then, for each ion in each system, the simulation process was repeated 10 times each time for 1ns, and PMF energy was determined from the average of the results obtained from the ten simulations. The pulling force of harmonic constraint is 10 Kcal/mol. Å was pulled to 15Å along z axis to point Z=0, that the position of membrane pore. Fig. 11 represents the average value of PMF for heavy metal ions, chlorine and water molecule in differently designed models. The figure also shows that water molecules had the lowest PMF value of about 7.3 to 14.7 Kcal/mol when passing through pores in all models. Therefore, water molecules could pass through the pores easily with the lowest resistance. In pristine SiC system with larger pores than functionalized membranes, water molecules passed the pores with the minimum PMF value of 7.3 Kcal/mol. In SiC@OH modified membranes, despite smaller diameter which inevitably results in higher energy barrier for water molecules, due to the existence of OH functional group, the value of PMF was not much different from that of SiC membranes with larger pores; i.e., water molecules passed SiC@OH pores with lowest energy barrier. This property is an excellent advantage of decorating SiC membrane pores with -OH functional group. Also, the ease of passage of water molecules from SiC@F pores with PMF=10.11 Kcal/mol was higher than that of SiC@N with PMF=14.67 Kcal/mol.

This procedure was repeated for all Cd^{2+}, Pb^{2+}, Zn^{2+} and Cl^{1-} ions.

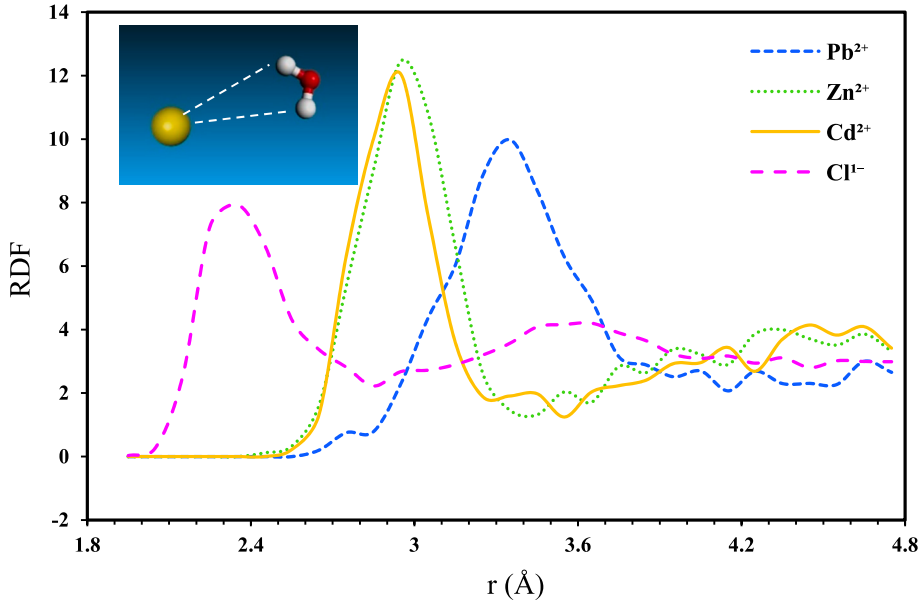

Fig. 9. The RDF of heavy metal ions from water molecules in contaminated water

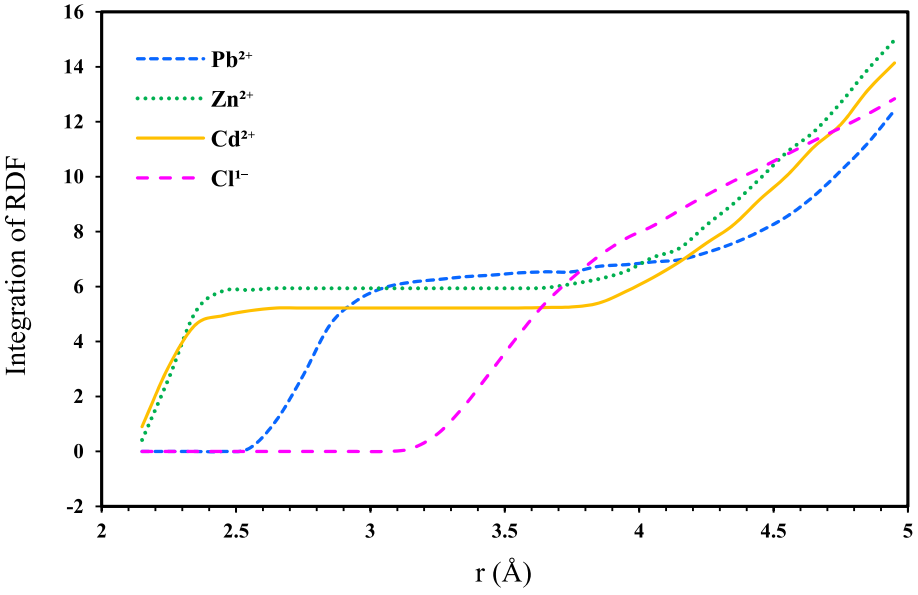

Fig. 10. The integration of RDF between heavy metal ions and water molecules

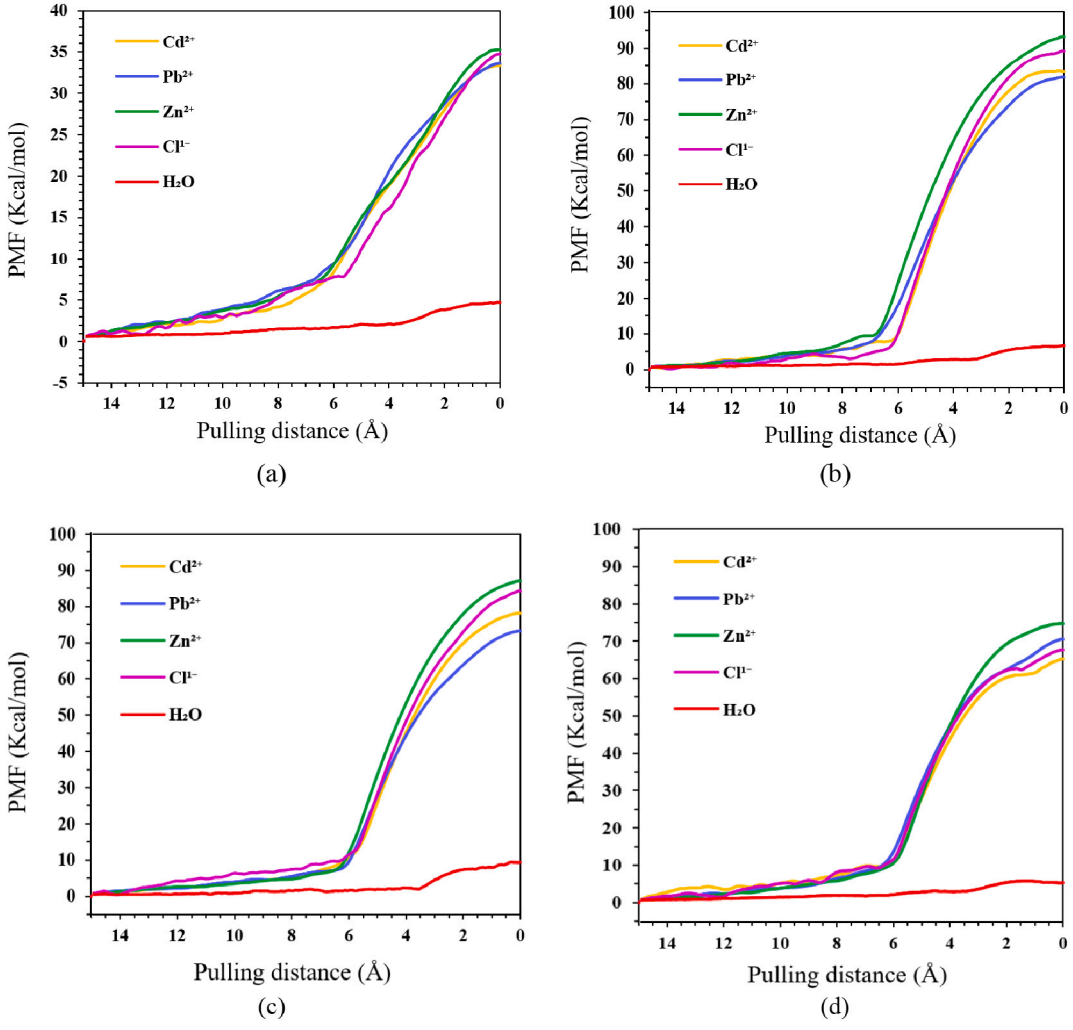

Fig. 11. PMF of heavy metals, chlorine and water molecule in (a) pristine SiC (b) SiC@F (c) SiC@N (d) SiC@OH

According to Fig. 11, PMF values of ions in functionalized pore systems were more than 2 times that of pristine pore SiC membrane with PMF value of 35 Kcal/mol. Higher forces were required for the passage of ions through the pores of functionalized membranes due to stronger electrostatic and Van der Waals interactions among functional atoms of pore edges (with different partial charges) and ions. Also, the effect of pore diameter could not be neglected. Ion PMF curves showed that selective ion rejection property of functionalized pores was higher than pristine SiC pores. For example, in pores of SiC@F and SiC@N, ion rejection order was Zn^{2+} >Cl^{1-} >Cd^{2+} >Pb^{2+} which complied with the results obtained in Fig. 6 for selective ion rejection. PMF analysis results proved that the PMF values of metal ions were in the following comparative order: SiC@F>SiC@N>SiC@OH>SiC.

3.6. Effect of temperature on water flux and ion rejection

In this section, 5 new simulations were performed to investigate the effect of temperature variation on flux and ion rejection capabilities. Main simulation conditions were 100 MPa pressure and 298K temperature. Considering fixed pressure of 100 MPa for 5 other systems, we examined the simulation at different temperatures of the systems with 20 K intervals from 278 to 378 K. as shown in Fig. 12, by increasing temperature from 278 to 378 K, due to lower water viscosity in higher temperature, increase of water flux was observed for all systems such that corresponding values for SiC, SiC@F, SiC@N and SiC@OH systems presented 18, 17.6, 17.6 and 22%, respectively. With deeper look at the figure, it was seen that the linear increasing trend of flux for functionalized membranes was observed to up to 358 K after which it remained almost constant. However, in pristine membrane, this increase occurred linearly to up to boiling point at 378 K. The reason for this could be larger pores in such membranes the permeation barriers of which could not overcome the high mobility of water molecules when approaching boiling temperature. In systems with functionalized membranes, due to smaller pores and higher permeation resistance, water molecules could not permeate more at temperatures higher than 358 K, so increasing trend of water flux remained almost constant. It can also be seen that the difference in the amount of flux for the three functionalized SiC models simulated at 298 K (ambient temperature) was low compared to higher temperatures. Due to differences in pore diameter, the amount of pore size expansion, under the effect of temperature rising was different. So, It could be concluded that the effect of pore size on flux for higher temperatures was more pronounced. Recently, a similar theory has been obtained [93].

Fig. 13 shows ion rejection percentages of recent systems versus temperature increase. Similar to previous sections, it was also witnessed that temperature increase significantly decreased ion rejection in all systems. This decrease in separation capability for SiC, SiC@F, SiC@N, and SiC@OH systems was 18, 8.7, 1 and 6.8 %, respectively. As could be seen, the system with SiC@N membrane presented the weakest effect on ion separation capability (almost none) with temperature increase. However, in the system with pristine membrane, temperature increase had the maximum effect on the decrease of ion rejection. Remaining systems containing functionalized membranes presented minor reduction in ion rejection efficiency for temperature higher than 318 °C. Therefore, it could be concluded that the ion rejection capability of functionalized membrane was almost independent of temperature increase.

Fig. 14 shows water flux variations during 5 ns of simulation for selected pristine SiC system at different temperatures. With a close look at the beginning of the diagram, it was found that, before moving the piston, increase of temperature increased kinetic energy and collision of water molecules, increasing the number of permeated water molecules from 343 to 645. This trend was continued until the end of simulation such that at the end of simulation, increase of temperature from 278 to 378 K resulted in the passage of 18% more water molecules.

3.7. Effect of electric field on water flux and ion rejection

In this section, the effect of electric field at different voltages on water flux and ion rejection was investigated. Also, in many studies, application of electric field for increasing ion permeation through membrane pores have been employed. However, in this work, we tested electric field application to hinder the permeation of ions through membrane pores. Therefore, we applied voltages of 0, 50, 10, 200, and 300 mV/Å along opposite direction of piston movement along z-axis on contaminated water. The range of applied voltage utilized in this study was similar to other experimental works in which the electric field was applied for the separation of heavy metals [94]. By observing simulation trajectory, we found that ions with positive charges tended to move along the direction of electric field. Similar results were obtained in [95]. Fig. 15 shows water flux at all applied voltages. As was seen, water flux at applied voltage of 50 mV/Å showed different behaviors in different models. In system with pristine SiC, flux remained constant, in those with SiC@F and SiC@N membranes corresponding value was

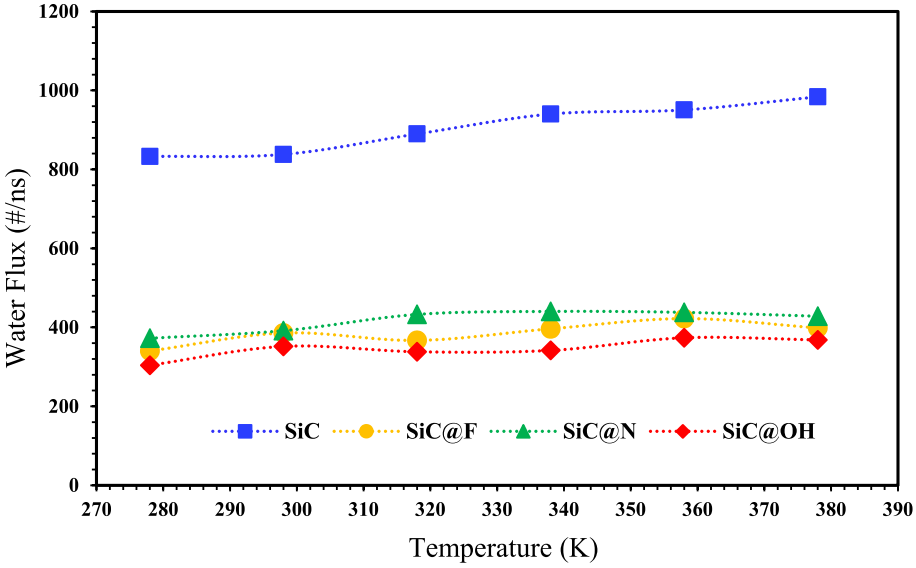

Fig. 12. Water Flow rate through SiC membranes at different temperatures

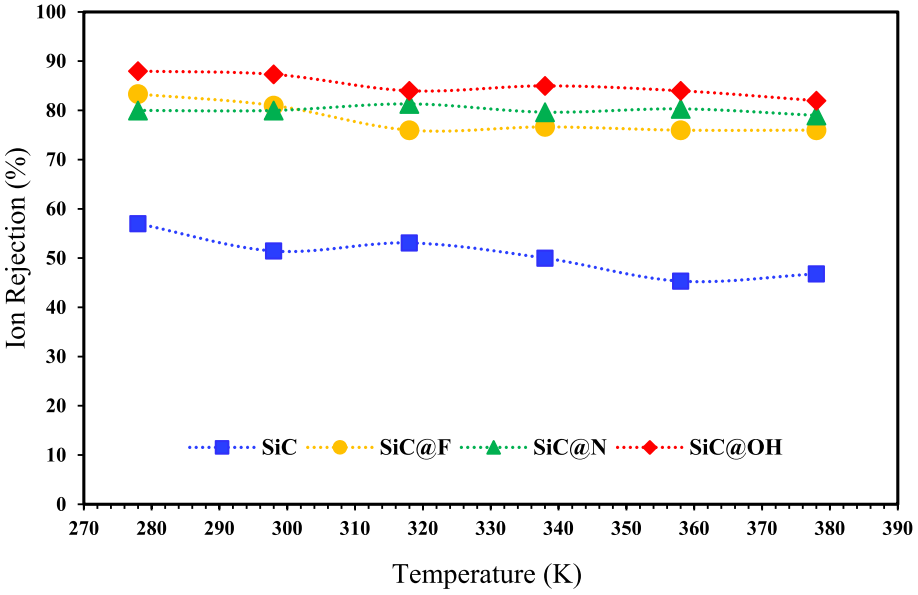

Fig. 13. Total Ion rejection percentage through different SiC membranes at different temperatures

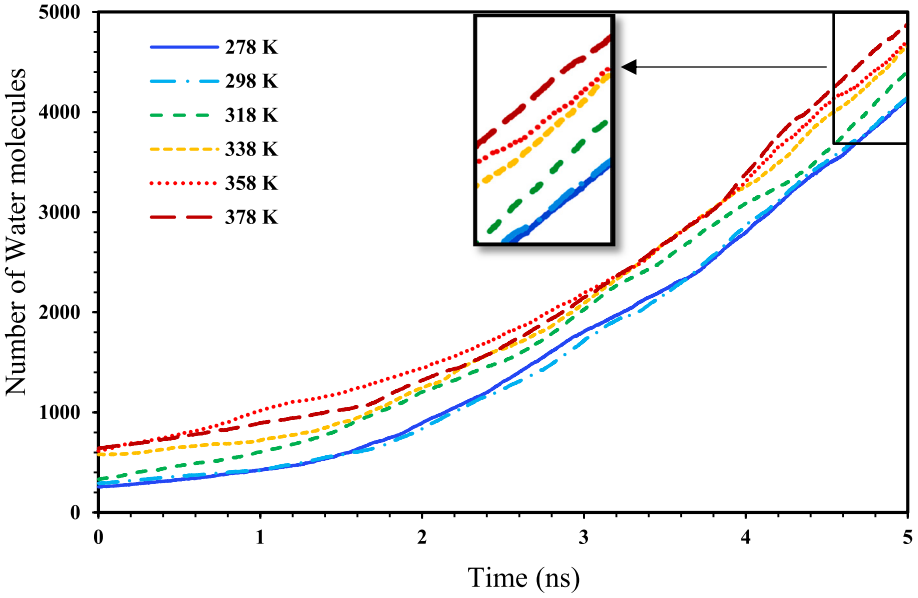

Fig. 14. Number of water molecules permeated through pristine SiC membrane versus simulation time at different temperatures

increased by 5% and 7%, respectively, and in the system with SiC@OH membrane it was decreased by about 14%. The reason for this difference in water permeation was differences in partial charge and electronic properties of functional groups on pore edges of SiC membrane where energy barrier was changed in the presence of electric field. Then, by applying higher voltages than 50 mV/Å, water flux was linearly decreased to 240.6 #/ns in pristine SiC membrane. However, in systems with functionalized membranes, linear decrease was continued to 200 mV/Å and remained constant after 123.2 #/ns for SiC@N and 101 #/ns for SiC@F and SiC@OH.

According to Fig. 16, one could claim that, like flux, application of voltage had different effect on the ion rejection of systems. Here also, up to 50 mV/Å, ion rejection remained constant in SiC@N membrane and in SiC@F and SiC@OH membranes, it was decreased by about 4% and 5%, respectively. However, the system with pristine SiC membrane presented about 18% improvement in ion rejection. Here also, increase of applied voltage to up to 300 mV/Å linearly improved ion rejection in pristine SiC membrane by up to 93.7%. However, in systems with functionalized membranes, maximum ion rejection improvement occurred at lower voltage of 200 mV/Å, at which more than 98% of ions were rejected, indicating 20% higher ion rejection compared to the situation with no applied voltage, which is a reasonable conclusion. Consequently, electric field had a significant effect on the control of water flux and performance of systems in the separation of heavy meatal ion in pristine and functionalized SiC membranes.

4. Conclusion

In this research, MD simulations were conducted using DFT calculations to study the separation of heavy metal ions Zn^{2+}, Pb^{2+} and Cd^{2+} in wastewater samples using porous SiC membranes under reverse osmosis pressure. The tests were performed on four models, including

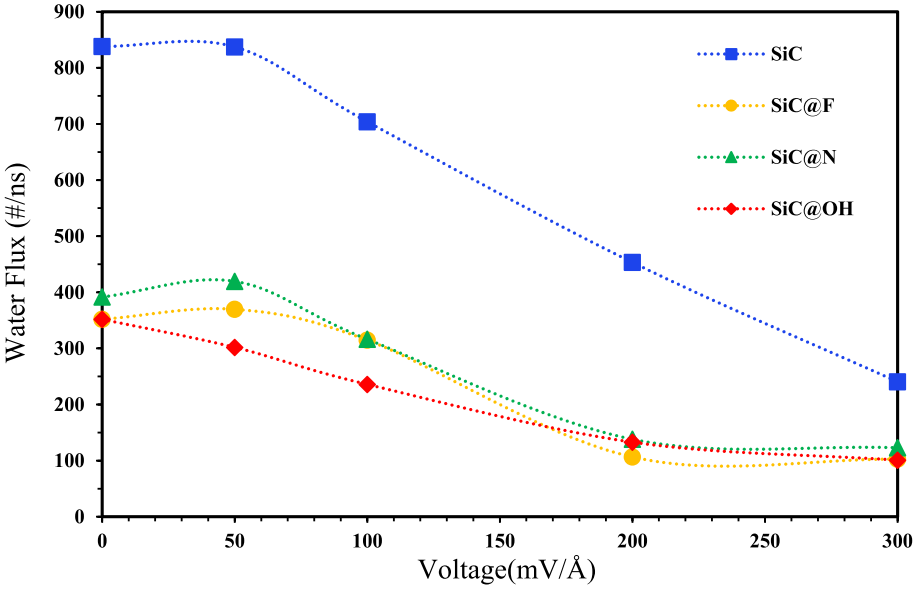

Fig. 15. Water flow rate through SiC membranes at different applied electric voltages (mV/Å)

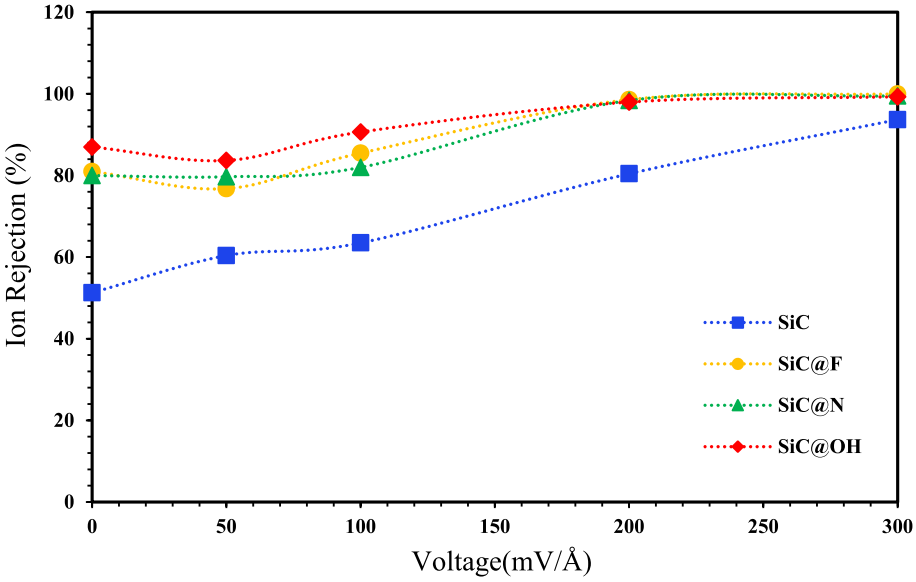

Fig. 16. Total ion rejection percentage through different SiC membranes at different applied electric voltages (mV/Å)

pristine SiC membrane as well as functionalized SiC with F, N and OH functional groups. Water molecules in all models were able to permeate pores. Water flux was increased with the increase of pressure which was directly related to pore diameter. Functionalization of SiC pores increased the system's ion rejection efficiency, and metal ions presented different pore permeation behavior in functionalized pores than that in pristine ones (selective separation ability). Therefore, pore edge engineering using different atoms could control their diameter, flux and ion rejection. Concentration profiles showed that water molecules beside membrane tended to accumulate, which was maximum and minimum in SiC@OH and pristine SiC membranes, respectively. RDF analyses showed that Zn^{2+} and Cd^{2+} ions had strong interactions with hydrogen atoms of water molecules at the distance of 3Å, which resulted in more accumulation of water molecules and higher resistance when permeating through pores. Integration of this RDF analysis showed that 5-6 water molecules surrounded metal ions. PMF calculations showed that metal ions required more than 2 times higher energy barrier to pass through functionalized pores of SiC membrane. Maximum energy barrier was obtained for Zn^{2+} ion, which presented high ion rejection on the membrane. The value of PMF for water molecules was very low, which indicated their simpler permeation through pores such that in SiC@OH systems, despite smaller pore diameter, it was about 2.5 times that in pristine SiC membrane; however, both membranes had almost similar MPF values.

In summary, the order of PMF values of metal ions for permeation was SiC@F>SiC@N>SiC@OH>SiC. Also, increase of temperature increased water flux and decreased ion rejection. In addition, we investigated the effect of applied voltage from 50 to 300 mV/Å in different systems and found that increase of voltage decreased water flux and increased ion rejection which was observed for functionalized membranes to up to 200 mV/Å, at which about 99% ion rejection was witnessed. Consequently, based on the obtained results, we concluded that electric field played an important role in designing systems for the separation of heavy metal ions. Finally, we noted that further

experimental studies are essential to advance the application of SiCs membranes in the practical water purification application.

Uncited references

[32,33]

Declaration of competing interest

The authors declare that they have no known competing financial interests or personal relationships that could have appeared to influence the work reported in this paper.

Acknowledgement

The authors would like to acknowledge the financial support from Global Excellence Statue (GES) Fellowship and National Research Foundation (NRF) of South Africa. Also, computation platforms were provided by Center of High Performance Computing (CHPC) at Cape Town and University of Johannesburg IT service which is gracefully acknowledged.

References

[1] E. Eray, V. Boffa, M.K. Jørgensen, G. Magnacca, V.M. Candelario, Enhanced fabrication of silicon carbide membranes for wastewater treatment: From laboratory to industrial scale, J. Membr. Sci. 606 (2020), https://doi.org/10.1016/j.memsci.2020.118080.

[2] M. Sun, X. Wang, L.R. Winter, Y. Zhao, W. Ma, T. Hedtke, J.-H. Kim, M. Elimelech, Electrified membranes for water treatment applications, ACS ES&T Eng. 1 (2021), https://doi.org/10.1021/acsestengg.1c00015.

[3] M. Kuhn, A. Bakshi, E. Sheridan, F. Rodrigues, A. Vincent, M. Moeller, R. Neufert, Silicon carbide membranes for water filtration applications in: Ceramics for Environmental Systems, John Wiley Sons, New Jersey, 2016.

[4] W. Cheng, J. Ma, X. Zhang, M. Elimelech, Sub-1 μm free-standing symmetric membrane for osmotic separations, Environ. Sci. Technol. Lett. (2019), https://doi.org/10.1021/acs.estlett.9b00364.

[5] Z. Wang, T. Horseman, A.P. Straub, N.Y. Yip, D. Li, M. Elimelech, S. Lin, Pathways and challenges for efficient solar-thermal desalination, Sci. Adv. 5 (2019) eaax0763, https://doi.org/10.1126/sciadv.aax0763.

[6] H. Li, T.-J.J. Ko, M. Lee, H.-S.S. Chung, S.S. Han, K.H. Oh, A. Sadmani, H. Kang, Y. Jung, Experimental realization of few layer two-dimensional mos 2 membranes of near atomic thickness for high efficiency water desalination, Nano Lett. 19 (2019) 5194–5204, https://doi.org/10.1021/acs.nanolett.9b01577.

[7] M. Qasim, M. Badrelzaman, N.N.A. Darwish, N.N.A. Darwish, N. Hilal, Reverse osmosis desalination: a state-of-the-art review, Desalination. 459 (2019) 59–104, https://doi.org/10.1016/j.desal.2019.02.008.

[8] C. Fritzmann, J. Löwenberg, T. Wintgens, T. Melin, State-of-the-art of reverse osmosis desalination, Desalination. 216 (2007) 1–76, https://doi.org/10.1016/j.desal.2006.12.009.

[9] M. Elimelech, W.A. Phillip, The future of seawater desalination: energy, technology, and the environment, Science (2011), https://doi.org/10.1126/science.1200488, 80-.

[10] H.M. Park, K.Y. Jee, Y.T. Lee, Preparation and characterization of a thin-film composite reverse osmosis membrane using a polysulfone membrane including metal-organic frameworks, J. Membr. Sci. 541 (2017), https://doi.org/10.1016/j.memsci.2017.07.034.

[11] W. Choi, S. Jeon, S.J. Kwon, H. Park, Y.I. Park, S.E. Nam, P.S. Lee, J.S. Lee, J. Choi, S. Hong, E.P. Chan, J.H. Lee, Thin film composite reverse osmosis membranes prepared via layered interfacial polymerization, J. Membr. Sci. 527 (2017), https://doi.org/10.1016/j.memsci.2016.12.066.

[12] A. Al Mayyahi, Important approaches to enhance reverse osmosis (RO) thin film composite (TFC) membranes performance, Membranes 8 (2018), https://doi.org/10.3390/membranes8030068. Basel.

[13] K.P. Lee, T.C. Arnot, D. Mattia, A review of reverse osmosis membrane materials for desalination - development to date and future potential, J. Membr. Sci. (2011), https://doi.org/10.1016/j.memsci.2010.12.036.

[14] S. Moazzem, J. Wills, L. Fan, F. Roddick, V. Jegatheesan, Performance of ceramic ultrafiltration and reverse osmosis membranes in treating car wash wastewater for reuse, Environ. Sci. Pollut. Res. 25 (2018) 8654–8668, https://doi.org/10.1007/s11356-017-1121-9.

[15] Z. Yang, Y. Zhou, Z. Feng, X. Rui, T. Zhang, Z. Zhang, A review on reverse osmosis and nanofiltration membranes for water purification, Polymers (Basel). 11 (2019), https://doi.org/10.3390/polym11081252.

[16] R. Wang, D. Chen, Q. Wang, Y. Ying, W. Gao, L. Xie, Recent advances in applications of carbon nanotubes for desalination: a review, Nanomater. 10 (2020) 1203, https://doi.org/10.3390/NANO10061203. Page 1203.

[17] R. Moradi-Dastjerdi, K. Behdinan, Free vibration response of smart sandwich plates with porous CNT-reinforced and piezoelectric layers, Appl. Math. Model. 96 (2021) 66–79, https://doi.org/10.1016/J.APM.2021.03.013.

[18] L. Liu, Y. Liu, Y. Qi, M. Song, L. Jiang, G. Fu, J. Li, Hexagonal boron nitride with nanoslits as a membrane for water desalination: A molecular dynamics investigation, Sep. Purif. Technol. 251 (2020), 117409, https://doi.org/10.1016/J.SEPPUR.2020.117409.

[19] Y.A.J. Al-Hamadani, B.M. Jun, M. Yoon, N. Taheri-Qazvini, S.A. Snyder, M. Jang, J. Heo, Y. Yoon, Applications of MXene-based membranes in water purification: a review, Chemosphere. 254 (2020), 126821, https://doi.org/10.1016/J.CHEMOSPHERE.2020.126821.

[20] P.O. Oviroh, T.-C. Jen, J. Ren, L.M. Mohlala, R. Warmbier, S. Karimzadeh, Nanoporous MoS2 membrane for water desalination: a molecular dynamics study, Langmuir. 37 (2021) 7127–7137, https://doi.org/10.1021/ACS.LANGMUIR.1C00708.

[21] R.E. Apreutesei, C. Catrinescu, C. Teodosiu, Surfactant-modified natural zeolites for environmental applications in water purification, Environ. Eng. Manag. J. 7 (2008) 149–161, https://doi.org/10.30638/EEMJ.2008.025.

[22] B.E. Logan, M. Elimelech, Membrane-based processes for sustainable power generation using water, Nature. 488 (2012), https://doi.org/10.1038/nature11477.

[23] S. Chabi, K. Kadel, Two-dimensional silicon carbide: emerging direct band gap semiconductor, Nanomater. Vol. 10 (2020) 2226, https://doi.org/10.3390/NANO10112226.

[24] T. Susi, V. Skákalová, A. Mittelberger, P. Kotrusz, M. Hulman, T.J. Pennycook, C. Mangler, J. Kotakoski, J.C. Meyer, Computational insights and the observation of SiC nanograin assembly: towards 2D silicon carbide, Sci. Report. 71 (7) (2017) 1–9, https://doi.org/10.1038/s41598-017-04683-9.

[25] Z. He, Z. Lyu, Q. Gu, L. Zhang, J. Wang, Ceramic-based membranes for water and wastewater treatment, Colloids Surfaces A Physicochem. Eng. Asp. 578 (2019), https://doi.org/10.1016/j.colsurfa.2019.05.074.

[26] P.S. Goh, A.F. Ismail, A review on inorganic membranes for desalination and wastewater treatment, Desalination. 434 (2018), https://doi.org/10.1016/j.desal.2017.07.023.

[27] S.G. Lehman, L. Liu, Application of ceramic membranes with pre-ozonation for treatment of secondary wastewater effluent, Water Res. 43 (2009), https://doi.org/10.1016/j.watres.2009.02.003.

[28] B. Hofs, J. Ogier, D. Vries, E.F. Beerendonk, E.R. Cornelissen, Comparison of ceramic and polymeric membrane permeability and fouling using surface water, Sep. Purif. Technol. 79 (2011), https://doi.org/10.1016/j.seppur.2011.03.025.

[29] M.C. Fraga, S. Sanches, J.G. Crespo, V.J. Pereira, Assessment of a new silicon carbide tubular honeycomb membrane for treatment of olive mill wastewaters, Membranes (Basel). 7 (2017), https://doi.org/10.3390/membranes7010012.

[30] L. Wang, N. Imanaka, W.M. Kriven, M. Fukushima, G. Kale, Ceramic for Environmental Systems (2016), https://doi.org/10.1002/9781119234463.

[31] R. Jafarzadeh, J. Azamat, H. Erfan-Niya, Water desalination across functionalized silicon carbide nanosheet membranes: insights from molecular simulations, Struct. Chem. 31 (2020) 293–303, https://doi.org/10.1007/S11224-019-01405-X.

[32] E. Eray, V.M. Candelario, V. Boffa, H. Safafar, D.N. Østedgaard-Munck, N. Zahrtmann, H. Kadrispahic, M.K. Jørgensen, A roadmap for the development and applications of silicon carbide membranes for liquid filtration: Recent advancements, challenges, and perspectives, Chem. Eng. J. 414 (2021), https://doi.org/10.1016/j.cej.2021.128826.

[33] T. Nagano, K. Sato, K. Kawahara, Gas permeation property of silicon carbide membranes synthesized by counter-diffusion chemical vapor deposition, Membranes 10 (2020), https://doi.org/10.3390/membranes10010011. Basel.

[34] M. Chen, R. Shang, P.M. Sberna, M.W.J. Luiten-Olieman, L.C. Rietveld, S.G. J. Heijman, Highly permeable silicon carbide-alumina ultrafiltration membranes for oil-in-water filtration produced with low-pressure chemical vapor deposition, Sep. Purif. Technol. 253 (2020), https://doi.org/10.1016/j.seppur.2020.117496.

[35] E.A. Filatova, D. Hausmann, S.D. Elliott, Investigating routes toward atomic layer deposition of silicon carbide: Ab initio screening of potential silicon and carbon precursors, J. Vac. Sci. Technol. A Vacuum, Surfaces, Film. 35 (2017), https://doi.org/10.1116/1.4964890.

[36] S.M. George, Atomic layer deposition: an overview, Chem. Rev. 110 (2010) 111–131, https://doi.org/10.1021/cr900056b.

[37] M. Aramesh, Y. Mayamei, A. Wolff, K. (Ken) Ostrikov, Superplastic nanoscale pore shaping by ion irradiation, Nat. Commun. 91 (9) (2018) 1–8, https://doi.org/10.1038/s41467-018-03316-7.

[38] N. Burham, A.A. Hamzah, B. YeopMajlis, Self-adjusting electrochemical etching technique for producing nanoporous silicon membrane, New Res. Silicon - Struct. Prop. Technol. (2017), https://doi.org/10.5772/67719.

[39] M.D. Fischbein, M. Drndić, Electron beam nanosculpting of suspended graphene sheets, Appl. Phys. Lett. 93 (2008), 113107, https://doi.org/10.1063/1.2980518.

[40] L. Liu, S. Ryu, M.R. Tomasik, E. Stolyarova, N. Jung, M.S. Hybertsen, M. L. Steigerwald, L.E. Brus, G.W. Flynn, Graphene oxidation: thickness-dependent etching and strong chemical doping, Nano Lett. 8 (2008) 1965–1970, https://doi.org/10.1021/NL0808684.

[41] F. Li, L. Li, X. Liao, Y. Wang, Precise pore size tuning and surface modifications of polymeric membranes using the atomic layer deposition technique, J. Membr. Sci. 385–386 (2011) 1–9, https://doi.org/10.1016/J.MEMSCI.2011.06.042.

[42] N.A. Renu, M. Agarwal, K. Singh, Methodologies for removal of heavy metal ions from wastewater: an overview, Interdiscip. Environ. Rev. 18 (2017) 124, https://doi.org/10.1504/IER.2017.087915.

[43] T. Yang, H. Lin, X. Zheng, K.P. Loh, B. Jia, Tailoring pores in graphene-based materials: from generation to applications, J. Mater. Chem. A 5 (2017) 16537–16558, https://doi.org/10.1039/C7TA04692H.
[44] S.M. Cohen, Modifying MOFs: new chemistry, new materials, Chem. Sci. 1 (2010) 32–36, https://doi.org/10.1039/C0SC00127A.
[45] L.H. Li Deepika, A.M. Glushenkov, S.K. Hait, P. Hodgson, Y. Chen, High-efficient production of boron nitride nanosheets via an optimized ball milling process for lubrication in oil, Sci. Report. 41 (4) (2014) 1–6, https://doi.org/10.1038/srep07288.
[46] J. Kotakoski, C.H. Jin, O. Lehtinen, K. Suenaga, A.V. Krasheninnikov, Electron knock-on damage in hexagonal boron nitride monolayers, Phys. Rev. B 82 (2010) 113404, https://doi.org/10.1103/PhysRevB.82.113404.
[47] J. C, L. F, S. K, I. S, Fabrication of a freestanding boron nitride single layer and its defect assignments, Phys. Rev. Lett. 102 (2009), https://doi.org/10.1103/PHYSREVLETT.102.195505.
[48] L. Xiao, D.M. Davenport, L. Ormsbee, D. Bhattacharyya, Polymerization and functionalization of membrane pores for water related applications, Ind. Eng. Chem. Res. 54 (2015) 4174–4182, https://doi.org/10.1021/IE504149T.
[49] D. Cohen-Tanugi, J.C. Grossman, Water desalination across nanoporous graphene, Nano Lett. 12 (2012) 3602–3608, https://doi.org/10.1021/NL3012853.
[50] D. Das, N. Kayal, G.A. Marsola, L.A. Damasceno, M.D. de M. Innocentini, Permeability behavior of silicon carbide-based membrane and performance study for oily wastewater treatment, Int. J. Appl. Ceram. Technol. 17 (2020), https://doi.org/10.1111/ijac.13463.
[51] P. de Wit, E.J. Kappert, T. Lohaus, M. Wessling, A. Nijmeijer, N.E. Benes, Highly permeable and mechanically robust silicon carbide hollow fiber membranes, J. Membr. Sci. 475 (2015), https://doi.org/10.1016/j.memsci.2014.10.045.
[52] M. Hosseini, J. Azamat, H. Erfan-Niya, Improving the performance of water desalination through ultra-permeable functionalized nanoporous graphene oxide membrane, Appl. Surf. Sci. 427 (2018), https://doi.org/10.1016/j.apsusc.2017.09.071.
[53] J. Azamat, N.B. Baghbani, H. Erfan-Niya, Atomistic understanding of functionalized γ-graphyne-1 nanosheet membranes for water desalination, J. Membr. Sci. 604 (2020), https://doi.org/10.1016/j.memsci.2020.118079.
[54] Y. Zhang, N.E. Almodovar-Arbelo, J.L. Weidman, D.S. Corti, B.W. Boudouris, W. A. Phillip, Fit-for-purpose block polymer membranes molecularly engineered for water treatment, Npj Clean Water. (2018), https://doi.org/10.1038/s41545-018-0002-1.
[55] M. Heiranian, A.B. Farimani, N.R. Aluru, Water desalination with a single-layer MoS 2 nanopore, Nat. Commun. 6 (2015) 1–6, https://doi.org/10.1038/ncomms9616.
[56] B. Zeuner, N. Ma, K. Berendt, A.S. Meyer, P. Andric, J.H. Jørgensen, M. Pinelo, Immobilization of alcohol dehydrogenase on ceramic silicon carbide membranes for enzymatic CH3OH production, J. Chem. Technol. Biotechnol. 93 (2018), https://doi.org/10.1002/jctb.5653.
[57] G. Cicero, A. Catellani, Towards SiC surface functionalization: an ab initio study, J. Chem. Phys. 122 (2005), https://doi.org/10.1063/1.1924546.
[58] A. Catellani, A. Calzolari, Functionalization of SiC(110) surfaces via porphyrin adsorption: ab initio results, J. Phys. Chem. C. 116 (2012), https://doi.org/10.1021/jp209072n.
[59] R. Qiu, S. Yuan, J. Xiao, X.D. Chen, C. Selomulya, X. Zhang, M.W. Woo, Effects of edge functional groups on water transport in graphene oxide membranes, ACS Appl. Mater. Interfaces 11 (2019) 8483–8491, https://doi.org/10.1021/ACSAMI.9B00492.
[60] H.W. Yoon, Y.H. Cho, H.B. Park, Graphene-based membranes: status and prospects, Philos. Trans. R. Soc. A Math. Phys. Eng. Sci. 374 (2016), https://doi.org/10.1098/RSTA.2015.0024.
[61] X.P. Li, G.P. Kong, X. Zhang, G.W. He, Pumping of water through carbon nanotubes by rotating electric field and rotating magnetic field, Appl. Phys. Lett. 103 (2013), https://doi.org/10.1063/1.4824441.
[62] K. Ritos, M.K. Borg, N.J. Mottram, J.M. Reese, Electric fields can control the transport of water in carbon nanotubes, Philos. Trans. R. Soc. A Math. Phys. Eng. Sci. 374 (2016), https://doi.org/10.1098/RSTA.2015.0025.
[63] J. Zhu, Y. Lan, H. Du, Y. Zhang, J. Su, Tuning water transport through nanochannels by changing the direction of an external electric field, Phys. Chem. Chem. Phys. 18 (2016) 17991–17996, https://doi.org/10.1039/C6CP00610H.
[64] J. Azamat, A. Khataee, S.W. Joo, Removal of heavy metals from water through armchair carbon and boron nitride nanotubes: a computer simulation study, RSC Adv. 5 (2015) 25097–25104, https://doi.org/10.1039/c4ra17048b.
[65] A. Kommu, S. Namsani, J.K. Singh, Removal of heavy metal ions using functionalized graphene membranes: A molecular dynamics study, RSC Adv. 6 (2016) 63190–63199, https://doi.org/10.1039/c6ra06817k.
[66] M. Rahimi, Z. Schoener, X. Zhu, F. Zhang, C.A. Gorski, B.E. Logan, Removal of copper from water using a thermally regenerative electrodeposition battery, J. Hazard. Mater. 322 (2017) 551–556, https://doi.org/10.1016/j.jhazmat.2016.10.022.
[67] Y. Li, Z. Xu, S. Liu, J. Zhang, X. Yang, Molecular simulation of reverse osmosis for heavy metal ions using functionalized nanoporous graphenes, Comput. Mater. Sci. 139 (2017) 65–74, https://doi.org/10.1016/j.commatsci.2017.07.032.
[68] P. Mark, L. Nilsson, Structure and dynamics of the TIP3P, SPC, and SPC/E water models at 298 K, J. Phys. Chem. A 105 (2001) 9954–9960, https://doi.org/10.1021/jp003020w.
[69] L. Martinez, R. Andrade, E.G. Birgin, J.M. Martínez, PACKMOL: A package for building initial configurations for molecular dynamics simulations, J. Comput. Chem. 30 (2009) 2157–2164, https://doi.org/10.1002/jcc.21224.
[70] E. Nazarparvar, M. Zahedi, E. Klein, Density functional theory (B3LYP) study of substituent effects on O-H bond dissociation enthalpies of trans -resveratrol derivatives and the role of intramolecular hydrogen bonds, J. Organomet. Chem. 77 (2012) 10093–10104, https://doi.org/10.1021/jo301612a.
[71] V.M. Frisch, G. Trucks, H. Schlegel, G. Scuseria, M. Robb, J. Cheeseman, G. Scalmani, G.P. Barone, B. Mennucci, Gaussian Inc., Wallingford CT, 2010 (n.d.).
[72] A.T. Steve Plimpton, Paul Crozier, LAMMPS-Large-Scale Atomic/Molecular Massively Parallel Simulator, 2007, p. 43.
[73] S. Karimzadeh, B. Safaei, T.C. Jen, Predicting phonon scattering and tunable thermal conductivity of 3D pillared graphene and boron nitride heterostructure, Int. J. Heat Mass Transf. 172 (2021), 121145, https://doi.org/10.1016/j.ijheatmasstransfer.2021.121145.
[74] W. Humphrey, A. Dalke, K. Schulten, VMD: Visual molecular dynamics, J. Mol. Graph. 14 (1996) 33–38, https://doi.org/10.1016/0263-7855(96)00018-5.
[75] J. Delhommelle, P. Millié, Inadequacy of the Lorentz-Berthelot combining rules for accurate predictions of equilibrium properties by molecular simulation, Mol. Phys. 99 (2001) 619–625, https://doi.org/10.1080/00268970010020041.
[76] U. Essmann, L. Perera, M.L. Berkowitz, T. Darden, H. Lee, L.G. Pedersen, A smooth particle mesh Ewald method, J. Chem. Phys. 103 (1995) 8577–8593, https://doi.org/10.1063/1.470117.
[77] J.K. Johnson, J.A. Zollweg, K.E. Gubbins, The Lennard-Jones equation of state revisited 78, 2006, pp. 591–618, https://doi.org/10.1080/00268979300100411, doi:10.1080/00268979300100411.
[78] E.A. Robinson, M.W. Lister, A Linear Relationship Between Bond Orders And Stretching Force Constants 41, 2011, pp. 2988–2995, https://doi.org/10.1139/V63-439 (doi:10.1139/V63-439).
[79] R.K. Mobley, Hydraulic fundamentals, in: Plant Eng. Handb, 2001, pp. 639–686, https://doi.org/10.1016/B978-075067328-0/50042-2.
[80] S. Park, K. Schulten, Calculating potentials of mean force from steered molecular dynamics simulations, J. Chem. Phys. 120 (2004) 5946–5961, https://doi.org/10.1063/1.1651473.
[81] L. Garnier, J. Devémy, C. Bonal, P. Malfreyt, Calculations of potential of mean force: application to ion-pairs and host–guest systems, Mol. Phys. 116 (2018) 1998–2008, https://doi.org/10.1080/00268976.2018.1442593.
[82] I. Buch, S.K. Sadiq, G. De Fabritiis, Optimized potential of mean force calculations for standard binding free energies, J. Chem. Theory Comput. 7 (2011) 1765–1772, https://doi.org/10.1021/ct2000638.
[83] S. Karimzadeh, B. Safaei, T.C. Jen, Prediction effect of ethanol molecules on doxorubicin drug delivery using single-walled carbon nanotube carrier through POPC cell membrane, J. Mol. Liq. 330 (2021), 115698, https://doi.org/10.1016/j.molliq.2021.115698.
[84] J. Gu, H. Li, X. Wang, A Self-Adaptive steered molecular dynamics method based on minimization of stretching force reveals the binding affinity of protein–ligand complexes, Mol. Vol. 20 (20) (2015) 19236–19251, https://doi.org/10.3390/MOLECULES201019236.
[85] S. Park, K. Schulten, Calculating potentials of mean force from steered molecular dynamics simulations, J. Chem. Phys. 120 (2004) 5946, https://doi.org/10.1063/1.1651473.
[86] S. Karimzadeh, B. Safaei, T.C. Jen, Investigate the importance of mechanical properties of SWCNT on doxorubicin anti-cancer drug adsorption for medical application: a molecular dynamic study, J. Mol. Graph. Model. 101 (2020), 107745, https://doi.org/10.1016/j.jmgm.2020.107745.
[87] K.H. Lee, U. Schnupf, B.G. Sumpter, S. Irle, Performance of density-functional tight-binding in comparison to ab initio and first-principles methods for isomer geometries and energies of glucose epimers in vacuo and solution, ACS Omega. 3 (2018) 16899–16915, https://doi.org/10.1021/acsomega.8b02213.
[88] E. Nemati-Kande, R. Karimian, V. Goodarzi, E. Ghazizadeh, Feasibility of pristine, Al-doped and Ga-doped boron nitride nanotubes for detecting SF4 gas: A DFT, NBO and QTAIM investigation, Appl. Surf. Sci. 510 (2020), 145490, https://doi.org/10.1016/j.apsusc.2020.145490.
[89] F. Mora, K. Pérez, C. Quezada, C. Herrera, A. Cassano, R. Ruby-Figueroa, Impact of membrane pore size on the clarification performance of grape marc extract by microfiltration, Membranes (Basel). 9 (2019), https://doi.org/10.3390/membranes9110146.
[90] Y.S. Polyakov, A.L. Zydney, Ultrafiltration membrane performance: effects of pore blockage/constriction, J. Membr. Sci. 434 (2013) 106–120, https://doi.org/10.1016/j.memsci.2013.01.052.
[91] K.J. Hwang, C.Y. Liao, K.L. Tung, Effect of membrane pore size on the particle fouling in membrane filtration, Desalination. 234 (2008) 16–23, https://doi.org/10.1016/j.desal.2007.09.065.
[92] A. Almojjly, D. Johnson, N. Hilal, Investigations of the effect of pore size of ceramic membranes on the pilot-scale removal of oil from oil-water emulsion, J. Water Process Eng. 31 (2019), 100868, https://doi.org/10.1016/j.jwpe.2019.100868.
[93] Z. Rizki, E. Suryawirawan, A.E.M. Janssen, A. van der Padt, R.M. Boom, Modelling temperature effects in a membrane cascade system for oligosaccharides, J. Membr. Sci. 610 (2020), 118292, https://doi.org/10.1016/J.MEMSCI.2020.118292.
[94] B.M. Pott, B. Mattiasson, Separation of heavy metals from water solutions at the laboratory scale, Biotechnol. Lett. 26 (2004) 451–456, https://doi.org/10.1023/B:BILE.0000018267.09698.cc.
[95] A. Lohrasebi, S. Rikhtehgaran, Ion separation and water purification by applying external electric field on porous graphene membrane, Nano Res. 11 (2018) 2229–2236, https://doi.org/10.1007/s12274-017-1842-6.